# Flatness-based control in successive loops for unmanned aerial vehicles and micro-satellites

G. Rigatos[a*] M. Abbaszadeh[b] K. Busawon[c] L. Dala[d]

[a]Unit of Industrial Autom.
Industrial Systems Institute
26504, Rion Patras Greece

[b]Department of ECSE
Rensselaer Polytechnic Inst.
12065, New York, USA

[c]Nonlinear Control Group
Univ. of Northumbria
Newcastle NE1 8ST, UK

[d]Dept. of Mech. Eng.
Univ. of Northumbria
Newcastle NE1 8ST, UK

**Abstract**: The control problem for the multivariable and nonlinear dynamics of unmanned aerial vehicles and micro-satellites is solved with the use of a flatness-based control approach which is implemented in successive loops. The state-space model of (i) unmanned aerial vehicles and (ii) micro-satellites is separated into two subsystems, which are connected between them in cascading loops. Each one of these subsystems can be viewed independently as a differentially flat system and control about it can be performed with inversion of its dynamics as in the case of input-output linearized flat systems. The state variables of the second subsystem become virtual control inputs for the first subsystem. In turn, exogenous control inputs are applied to the first subsystem. The whole control method is implemented in two successive loops and its global stability properties are also proven through Lyapunov stability analysis. The validity of the control method is confirmed in two case studies: (a) control and trajectories tracking for the autonomous octocopter, (ii) control of the attitude dynamics of micro-satellites.

**Keywords**: autonomous octocopter, attitude dynamics of micro-satellites, multivariable control, differential flatness properties, flatness-based control in successive loops, global stability, Lyapunov analysis.

## 1 Introduction

Differential flatness theory is a main research direction in the area of nonlinear dynamical systems [1-6]. A system is considered to be differentially flat if all its state variables and its control inputs can be expressed as functions of one single algebraic variable which is the so-called flat output, and also as functions of the flat-output's derivatives [7-10]. The differential flatness property enables the transformation of the nonlinear system's dynamics in the linear canonical form [11-15]. The latter description is controllable and observable thus allowing to treat effectively control and estimation problems [16-19]. In this paper, a successive loops approach is developed for controller design in nonlinear dynamical systems which exhibit the differential flatness property. The method makes use of the initial nonlinear model of the system and of its decomposition into a set of nonlinear subsystems for which the differential flatness property holds [20-26].

The article introduces a novel solution to the problem of nonlinear control of complex dynamical systems without the need to apply changes of state variables (diffeomorphisms) and complicated state-space transformations. The new solution is a flatness-based control approach implemented in successive loops. In this method the dynamic model of the nonlinear system is separated into subsystems which are connected in a cascading manner. This control method is directly applicable to dynamical systems of the triangular form and to nonlinear systems which can be transformed into such a form. The state-space model of the initial nonlinear system is decomposed into cascading subsystems which satisfy differential flatness properties.

*email: grigat@ieee.org

For each subsystem of the state-space model a virtual control input is computed, capable of inverting the subsystem's dynamics and of eliminating the subsystem's tracking error. The control input which is actually applied to the initial nonlinear system is computed from the last row of the state-space description. This control input incorporates in a recursive manner all virtual control inputs which were computed from the individual subsystems included in the initial state-space equation. The control input that should be applied to the nonlinear system so as to assure that all state vector elements will converge to the desirable setpoints is obtained at each iteration of the control algorithm by tracing backwards the subsystems of the state-space model.

The first application domain for the article's developments on flatness-based control in successive loops is multi-rotor Unmanned Aerial Vehicles. Octorotors are UAVs equipped with 8 rotors, which are usually placed at equidistant positions on the vertices of an octagon (star-shaped octorotors). Alternatively, there can be octocopters where the rotors are connected on a basis that comprises two orthogonal rods [27-29]. Octorotors can be used for surveillance, patrolling and defence tasks. They can function reliably under rough conditions and in environments which are difficult for humans to access [30-32]. Because of having a larger number of motors than tri-rotors and quadrotors they can transport heavier loads while also being more resilient against motors' failures [33-35]. The octorotor has six degrees of freedom, namely it can perform translational motion in the cartesian space, while it can also perform rotations by a yaw, pitch and roll angle around the axes of an inertial coordinates reference frame [36-38]. An octorotor receives four control inputs. These are the thrust provided by the rotors and three torques which result in the rotational motion of the UAV around the axes of the inertial reference system. The latter are the yaw, pitch and roll motion controls [39-41]. In turn these control inputs are determined by adjusting the power that is provided by the individual motors of the UAV [42 -44]. There exist several attempts towards the solution of the nonlinear multivariable control problem for octorotors. Global stability and robustness are the objectives that controllers' design for octorotors aims at achieving [45-48]. The developments of the present article in the octorotor control problem have been preceded by the results given in [49-50].

The second application domain for the article's developments of flatness-based control implemented in successive loops is the attitude control problem of micro-satellites. Attitude control for satellites is important for the precise orientation of theirs and consequently for assuring the reliable transmission of communication data or the accomplishment of image acquisition, navigation, geodesic and surveillance tasks [51-54]. Attitude control is applied to satellites to compensate for various space-environmental disturbances, as well as for inner moment-of-inertia variations [55- 58]. The Attitude Determination and Control Subsystem (ADCS) consists of various sensors and actuators which provide information about attitude and finally stabilize the satellite at the desirable orientation [59-61]. Control of the satellite's attitude can be accomplished by using as control inputs electromagnetic actuation, solar-powered actuation, reaction wheels as well as thrusters. The present article is particularly focusing on micro-satellites. These have usually mass that is less than 100Kg and thus their manufacturing is less costly, takes shorter time and has less failure risks. Micro-satellites have a significant role in navigation, earth observation, atmosphere data collection and tele-communications [62-64]. Unlike satellites of larger dimensions and weight that comprises flexible parts, micro-satellites can be described by the dynamics of a rigid body. Three-axis attitude control of micro-satellites requires the solution of a multi-variable and highly nonlinear control problem [65-67]. Elimination of the satellite's orientation error is the primary objective of an attitude control system. Besides, another important feature is robustness against the disturbances that may affect the satellite's control loop [68-70]. There have been several attempts to solve the satellite's attitude stabilization problem with the use of linear and nonlinear control techniques [71-73]. Although significant developments have been witnessed in nonlinear controllers design for the attitude control problem, this research area is still open. The developments of the present article in the satellite and aerospace systems control problem have been preceded by the results given in [74-75].

The structure of the paper is as follows: In Section 2 the dynamic model of the 6-DOF octocopter is ana-

lyzed. In Section 3 flatness-based control in successive loops is applied to the dynamic model of the 6-DOF octocopter UAV. In Section 4 the dynamic model of the 3-DOF micro-satellite is analyzed. In Section 5 flatness-based control in successive loops is applied to the 3-DOF dynamic model of the attitude of micro-satellites. In Section 6 simulation tests are presented about the performance of the flatness-based control method in successive loops when used (a) in the dynamic model of the 6-DOF autonomous octocopter, (b) in the 3-DOF dynamic model of the attitude of micro-satellites. Finally, in Section 7 concluding remarks are stated.

## 2 Dynamic model of the octocopter UAV

The diagram of the autonomous octocopter is shown in Fig. 1. The initial state-space form of the octocopter UAV is given by the 6-DOF model with state vector [8], [49]

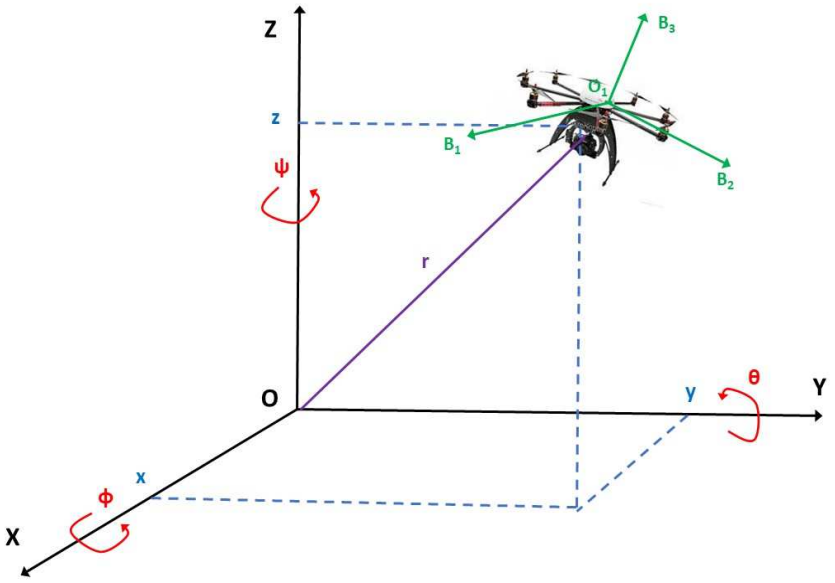


Figure 1: Diagram of the autonomous octorotor, and the associated body-fixed and inertial reference frames

$$x = [x_1, x_2, x_3, x_4, x_5, x_6, x_7, x_8, x_9, x_{10}, x_{11}, x_{12}]^T \text{ or}$$
$$x = [x, \dot{x}, y, \dot{y}, z, \dot{z}, \phi, \dot{\phi}, \theta, \dot{\theta}, \psi, \dot{\psi}]^T \quad (1)$$

where $(x, y, z)$ are the cartesian coordinates of the center of gravity of the drone and $(\phi, \theta, \psi)$ are Euler orientation angles expressed in the inertial reference frame $OXYZ$, while the state-space equations of the model are [8], [49]

$$
\begin{array}{c}
\dot{x}_1 = x_2 \\
\dot{x}_2 = \frac{U_1}{m}[sin(x_{11})sin(x_7) + cos(x_{11})sin(x_9)cos(x_7)] - \frac{K_{ft,x}}{m}x_2 \\
\dot{x}_3 = x_4 \\
\dot{x}_4 = \frac{U_1}{m}[-cos(x_{11})sin(x_7) + sin(x_{11})sin(x_9)cos(x_7)] - \frac{K_{ft,y}}{m}x_4 \\
\dot{x}_5 = x_6 \\
\dot{x}_6 = \frac{U_1}{m}[cos(x_9)cos(x_{11})] - \frac{K_{ft,z}}{m}x_6 \\
\dot{x}_7 = x_8 \\
\dot{x}_8 = \frac{I_y - I_z}{I_x}x_{10}x_{12} - \frac{I_{rotor}}{I_x}x_{10}\gamma - \frac{K_{fa,x}}{I_x}x_8^2 + \frac{LU_2}{I_x} \\
\dot{x}_9 = x_{10} \\
\dot{x}_{10} = \frac{I_z - I_x}{I_y}x_8x_{12} + \frac{I_{rotor}}{I_y}x_8\gamma - \frac{K_{fa,y}}{I_y}x_{10}^2 + \frac{LU_3}{I_y} \\
\dot{x}_{11} = x_{12} \\
\dot{x}_{12} = \frac{I_x - I_y}{I_z}x_8x_{10} - \frac{K_{fa,z}}{I_z}x_{12}^2 + \frac{U_4}{I_z}
\end{array}
\tag{2}
$$

In the last three rows of Eq. (2), $L$ the distance between the center of gravity of the octorotor and each motor. The control inputs of the system are $U_1$ which is the lift thrust and $U_2$, $U_3$, $U_4$ are the torques due to different rotation speeds of the motors which cause turn of the UAV around the OX.OY and OZ axis. By defining the control input variables

$$
\begin{array}{c}
v_1 = \frac{U_1}{m}[sin(x_{11})sin(x_7) + cos(x_{11})sin(x_9)cos(x_7)] \\
v_2 = \frac{U_1}{m}[-cos(x_{11})sin(x_7) + sin(x_{11})sin(x_9)cos(x_7)] \\
v_3 = \frac{U_1}{m}[cos(x_9)cos(x_{11})] - g \;\; v_4 = U_2 \;\;\; v_5 = U_3 \;\;\; v_6 = U_4
\end{array}
\tag{3}
$$

and using the property that

$$
U_1 = \sqrt{v_1^2 + v_2^2 + (v_3 + g)^2} \tag{4}
$$

the previous state-space model is rewritten as

$$
\begin{array}{c}
\dot{x}_1 = x_2 \\
\dot{x}_2 = -\frac{K_{ft,x}}{m}x_2 + v_1 \\
\dot{x}_3 = x_4 \\
\dot{x}_4 = -\frac{K_{ft,y}}{m}x_4 + v_2 \\
\dot{x}_5 = x_6 \\
\dot{x}_6 = -\frac{K_{ft,z}}{m}x_6 + v_3 \\
\dot{x}_7 = x_8 \\
\dot{x}_8 = \frac{I_y - I_z}{I_x}x_{10}x_{12} - \frac{I_{rotor}}{I_x}x_{10}\gamma - \frac{K_{fa,x}}{I_x}x_8^2 + \frac{Lv_4}{I_x} \\
\dot{x}_9 = x_{10} \\
\dot{x}_{10} = \frac{I_z - I_x}{I_y}x_8x_{12} + \frac{I_{rotor}}{I_y}x_8\gamma - \frac{K_{fa,y}}{I_y}x_{10}^2 + \frac{Lv_5}{I_y} \\
\dot{x}_{11} = x_{12} \\
\dot{x}_{12} = \frac{I_x - I_y}{I_z}x_8x_{10} - \frac{K_{fa,z}}{I_z}x_{12}^2 + \frac{v_6}{I_z}
\end{array}
\tag{5}
$$

For the state-space model of Eq. (5) a re-ordering of state-space variables is performed as follows

$$
\begin{array}{c}
z = [z_1, z_2, z_3, z_4, z_5, z_6, z_7, z_8, z_9, z_{10}, z_{11}, z_{12}]^T \text{ or} \\
z = [x, y, z, \phi, \theta, \psi, \dot{x}, \dot{y}, \dot{x}, \dot{\phi}, \dot{\theta}, \dot{\psi}]^T
\end{array}
\tag{6}
$$

the dynamics of the octocopter UAV is written in the following matrix form

$$\begin{pmatrix} \dot{z}_1 \\ \dot{z}_2 \\ \dot{z}_3 \\ \dot{z}_4 \\ \dot{z}_5 \\ \dot{z}_6 \\ \dot{z}_7 \\ \dot{z}_8 \\ \dot{z}_9 \\ \dot{z}_{10} \\ \dot{z}_{11} \\ \dot{z}_{12} \end{pmatrix} = \begin{pmatrix} z_7 \\ z_8 \\ z_9 \\ z_{10} \\ z_{11} \\ z_{12} \\ -\frac{K_{ft,x}}{m} z_7 \\ -\frac{K_{ft,y}}{m} z_8 \\ -\frac{K_{ft,z}}{m} z_9 \\ \frac{I_y - I_z}{I_x} z_{11} z_{12} - \frac{I_{rotor}}{I_x} z_{11}\gamma - \frac{K_{fa,x}}{I_x} z_{10}^2 \\ \frac{I_z - I_x}{I_y} z_{10} z_{12} + \frac{I_{rotor}}{I_y} z_{10}\gamma - \frac{K_{fa,y}}{I_y} z_{11}^2 \\ \frac{I_x - I_y}{I_z} z_{10} z_{11} - \frac{K_{fa,z}}{I_z} z_{12}^2 \end{pmatrix} + \begin{pmatrix} 0 & 0 & 0 & 0 & 0 & 0 \\ 0 & 0 & 0 & 0 & 0 & 0 \\ 0 & 0 & 0 & 0 & 0 & 0 \\ 0 & 0 & 0 & 0 & 0 & 0 \\ 0 & 0 & 0 & 0 & 0 & 0 \\ 0 & 0 & 0 & 0 & 0 & 0 \\ 1 & 0 & 0 & 0 & 0 & 0 \\ 0 & 1 & 0 & 0 & 0 & 0 \\ 0 & 0 & 1 & 0 & 0 & 0 \\ 0 & 0 & 0 & \frac{1}{I_x} & 0 & 0 \\ 0 & 0 & 0 & 0 & \frac{1}{I_y} & 0 \\ 0 & 0 & 0 & 0 & 0 & \frac{1}{I_z} \end{pmatrix} \begin{pmatrix} v_1 \\ v_2 \\ v_3 \\ v_4 \\ v_5 \\ v_6 \end{pmatrix} \tag{7}$$

By separating state vector $z$ into the following subvectors

$$\begin{aligned} z_a &= [z_1, z_2, z_3, z_4, z_5, z_6]^T \\ z_b &= [z_7, z_8, z_8, z_{10}, z_{11}, z_{12}]^T \end{aligned} \tag{8}$$

as well as the drift vectors

$$f_a(x) = [z_7, z_8, z_9, z_{10}, z_{11}, z_{12}]^T \tag{9}$$

$$\begin{aligned} f_b(x) = [&-\tfrac{K_{ft,x}}{m} z_7, -\tfrac{K_{ft,y}}{m} z_8, -\tfrac{K_{ft,z}}{m} z_9, \\ &\tfrac{I_y - I_z}{I_x} z_{11} z_{12} - \tfrac{I_{rotor}}{I_x} z_{11}\gamma - \tfrac{K_{fa,x}}{I_x} z_{10}^2, \\ &\tfrac{I_z - I_x}{I_y} z_{10} z_{12} + \tfrac{I_{rotor}}{I_y} z_{10}\gamma - \tfrac{K_{fa,y}}{I_y} z_{11}^2, \\ &\tfrac{I_x - I_y}{I_z} z_{10} z_{11} - \tfrac{K_{fa,z}}{I_z} z_{12}^2]^T \end{aligned} \tag{10}$$

and the control input gain matrices

$$g_a(x) = 0_{6\times 6} \tag{11}$$

$$g_b(x) = \begin{pmatrix} 1 & 0 & 0 & 0 & 0 & 0 \\ 0 & 1 & 0 & 0 & 0 & 0 \\ 0 & 0 & 1 & 0 & 0 & 0 \\ 0 & 0 & 0 & \frac{1}{I_x} & 0 & 0 \\ 0 & 0 & 0 & 0 & \frac{1}{I_y} & 0 \\ 0 & 0 & 0 & 0 & 0 & \frac{1}{I_z} \end{pmatrix} \tag{12}$$

the state-space model of the octocopter UAV comes in the following concise and also triangular state-space form

$$\begin{pmatrix} \dot{z}_a \\ \dot{z}_b \end{pmatrix} = \begin{pmatrix} f_a(x) \\ f_b(x) \end{pmatrix} + \begin{pmatrix} g_a(x) \\ g_b(x) \end{pmatrix} v \tag{13}$$

or equivalently the UAV's dynamics is decomposed into the following two subsystems

$$\dot{z}_a = z_b \tag{14}$$

$$\dot{z}_b = f_b(z) + g_b(z)v \tag{15}$$

It can be proven that the 6-DOF octocopter is a differentially flat system with flat output $y = z_a$. Indeed, from Eq. (14) one obtains

$$\dot{z}_a = z_b \Rightarrow z_b = \dot{y} \tag{16}$$

Thus $z_b$ is a differential function of the flat output $y$. Besides. in Eq. (15) one has that $f_b(z)$ is also a function of $y$ and $\dot{y}$ while $g_b(z)$ has elements with constant values. Thus, by solving Eq. (15) with respect to the control input $v$ one obtains

$$v = g_b(z)^{-1}[\dot{z}_b - f_b(z)] \tag{17}$$

therefore $v$ is also a differential function of the flat output $y$. As a result of the above the 6-DOF octocopter is a differentially flat system.

**Table Ia**

**Parameters of the octocopter's dynamic model**

| *Parameter* | *Definition* |
|---|---|
| $x, y, z$ | Cartesian coordinates of the UAV in the inertial frame |
| $\phi, \theta, \psi$ | Euler orientation angles relative to the inertial reference frame |
| $u, v, w$ | linear velocities of the UAV along the axes of the body-fixed frame |
| $p, q, r$ | Rotation speed around the axes of the body-fixed frame |
| $U_1$ | thrust (lift) force of the UAV |
| $U_2, U_3, U_4$ | torques that rotate the UAV around the axes of the inertial frame |
| $m$ | mass of the autonomous octocopter |
| $I_x, I_y, I_z$ | moments of inertia in rotation around the axes of tbe inertial frame |
| $L$ | distance between the center of gravity of the octorotor and each motor |
| $K_{ft,x}, K_{ft,y}, K_{ft,z}$ | friction coefficients for the linear motion of the UAV |
| $K_{fa,x}, K_{fa,y}, K_{fa,z}$ | friction coefficients for the rotational motion of the UAV |

## 3 Flatness-based control in successive loops for the octocopter UAV

The previously given Eq. (14) and Eq. (15) describe decomposition of the octocopter's dynamics into two subsystems which are both differentially flat. In Eq. (14) $z_a$ is taken to be the state vector and $z_b$ is taken to be the virtual control inputs vector. It holds that $z_b = \dot{z}_a$, thus the virtual control inputs vector is a differential function of the subsystem's flat outputs vector. Consequently, the subsystem of Eq. (14) is differentially flat.

For the subsystem of Eq. (15), $z_b$ is the flat outputs vector. Besides, the elements of state vector $z_a$ are now viewed as coefficients. Thus, $f_a(z)$ and $g_a(z)$ are also functions of the flat outputs vector $z_b$. Additionally, using Eq. (17) one has that $v$ is a differential function of $z_b$. Consequently, the subsystem of Eq. (15) is also differentially flat.

Next, the control of the subsystem of Eq. (14) and of the subsystem of Eq. (15) can be carried out following the design process of controllers for input-output linearized differentially flat systems. For the subsystem of Eq. (14) the setpoints vector is defined as $z_a^d$ and the values of the virtual control input which stabilize the subsystem's dynamics are given by

$$z_b^* = \dot{z}_a^d - K_1(z_a - z_a^d) \tag{18}$$

Matrix $K_1 \in R^{6\times 6}$ is a diagonal matrix with elements $k_{ii} > 0$ for $i = 1, 2, \cdots, 6$. For the subsystem of Eq. (15) the control inputs vector $v$ is selected so as to assure that the subsystem's state vector $z_b$ will converge

to the targeted value $z_b^*$ that makes in turn the state vector of the subsystem of Eq. (14) converge to its associated setpoint. The setpoint for the second subsystem is $z_b^d = z_b^*$ and the control input $v$ is given by

$$v = g_b^{-1}(z)[\dot{z}_b^d - f_b(z) - K_2(z_b - z_b^d)] \tag{19}$$

Matrix $K_2 \in R^{6\times 6}$ is a diagonal matrix with elements $k_{ii} > 0$, $i = 1, 2, \cdots, 6$. Next, by substituting Eq. (18) into Eq. (14) and Eq. (19) into Eq. (15) one obtains the octocopter's closed-loop dynamics, which is given by

$$\begin{array}{c}(\dot{z}_a - \dot{z}_a^d) + K_1(z_a - z_a^d) = 0 \\ (\dot{z}_b - \dot{z}_b^d) + K_2(z_b - z_b^d) = 0\end{array} \tag{20}$$

or by defining the tracking error variables $e_a = z_a - z_a^d$ and $e_b = z_b - z_b^d$ one has

$$\begin{array}{c}\dot{e}_a + K_1 e_a = 0 \Rightarrow \lim_{t\to\infty} e_a(t) = 0 \Rightarrow \lim_{t\to\infty} z_a(t) = z_a^d(t) \\ \dot{e}_b + K_2 e_b = 0 \Rightarrow \lim_{t\to\infty} e_b(t) = 0 \Rightarrow \lim_{t\to\infty} z_b(t) = z_b^d(t)\end{array} \tag{21}$$

Consequently, all state variables of the 6-DOF octocopter converge to the associated setpoints, or equivalently $\lim_{t\to\infty} x_i(t) = x_i^d(t)$ for $i = 1, 2, \cdots, 12$. The global stability properties of flatness-based control in successive loops for the octocopter's model can be also proven through Lyapunov analysis. To this end, the following Lyapunov function is defined

$$V = \tfrac{1}{2}[e_a^T e_a + e_b^T e_b] \tag{22}$$

By differentiating $V$ in time and with the use of Eq. (21) one obtains

$$\begin{array}{c}\dot{V} = e_a^T \dot{e}_a + e_b^T \dot{e}_b \Rightarrow \dot{V} = e_a^T(-K_1 e_a) + e_b^T(-K_2 e_b) \Rightarrow \\ \dot{V} = -e_a^T K_1 e_a - e_b^T K_2 e_b \Rightarrow \dot{V} < 0\end{array} \tag{23}$$

It holds that $\dot{V}$ is strictly negative $\forall e_a \neq 0$ and $\forall e_b \neq 0$. It becomes 0 only when $e_a = 0$ and $e_b = 0$. Therefore, the Lyapunov function of the system is strictly diminishing and finally converges to 0, no matter what the initial conditions of the UAV's tracking error are. Thus, the control loop of the octocopter UAV is globally asymptotically stable.

Therefore, $V$ is a strictly diminishing function which converges asymptotically to 0. Consequently, it holds that $lim_{t\to\infty} e_{1,6} = 0$ and $lim_{t\to\infty} e_{7,12} = 0$.

An explicit demonstration of the exponential stabilization that is achieved by flatness-based control in successive loops is given next. The Lyapunov function of the control loop is written as:

$$V = \tfrac{1}{2}[\textstyle\sum_{i=1}^{6} e_i^2 + \sum_{j=7}^{12} e_j^2] \tag{24}$$

where $e_i$ $i = 1, \cdots, 6$ are the tracking errors for the state variables of the octocopter associated with the first subsystem and $e_j$ $j = 7, \cdots, 12$ are the tracking errors for the state variables of the octocopter associated with the second subsystem. Equivalently, the first-order time-derivative of the Lyapunov function is written as

$$\dot{V} = -[\textstyle\sum_{i=1}^{6} k_{1,i} e_i^2 + \sum_{j=7}^{12} k_{2,j-6} e_j^2] \tag{25}$$

where $k_{1,i} > 0$ $i = 1, \cdots, 6$ are the diagonal elements of gain matrix $K_1$ and $k_{2,j-6} > 0$ $j = 7, \cdots, 12$ are the diagonal elements of gain matrix $K_2$. By denoting the minimum of the above-noted elements of the feedback gain matrices as $k_{min}$, that is

$$k_{min} = min\{k_{1,i} :\ i = 1, \cdots, 6 \text{ and } k_{2,j-6} :\ j = 7, \cdots, 12\} \tag{26}$$

and using Eq. (25) one obtains that

$$\begin{array}{c} \dot{V} \leq -k_{min}[\sum_{i=1}^{6} e_i^2 + \sum_{j=7}^{12} e_j^2] \\ \Rightarrow \dot{V} \leq -2k_{min} V \Rightarrow \dot{V} + 2k_{min} V \leq 0 \end{array} \tag{27}$$

From Eq. (27) one can demonstrate the exponential convergence of the Lyapunov function $V$ to 0.

The feedback control scheme, which is followed for the cascading subsystems that constitute the dynamic model of the 6-DOF octocopter and which is based on inversion of the subsystems' dynamics of this aerial drone, is equally robust to sliding-mode control in which the switching control term has been substituted by a saturation function. One can easily confirm this for the first-order $i$-th subsystem of the form $\dot{x}_i = f_i(x_i) + g_i(x_i)v_i$ by defining the sliding surface $s_i = e_i = x_1 - x_i^d$ and the associated sliding mode controller $v_i = \hat{g}_i(x)^{-1}[\dot{x}_i^d - \hat{f}_i(x_i) - K_i sgn(x_i - x_i^d)]$ which after substituting the $sgn(s_i)$ function with the saturation $sat(s_i)$ function becomes $v_i = \hat{g}_i(x)^{-1}[\dot{x}_i^d - \hat{f}_i(x_i) - K_i(x_i - x_i^d)]$. The latter relation coincides with the flatness-based control in successive loops for the $i$-th subsystem under uncertainty (with use of the estimated functions $\hat{f}_i(x)$ and $\hat{g}_i(x)$) which is computed by the article's control method. Therefore, the proposed flatness-based control method in successive loops provides sufficient robustness margins which enable the reliable and safe functioning of the 6-DOF octocopter under reasonable levels of model uncertainty or external perturbations.

## 4 Dynamic model of the micro-satellite

The diagram of the micro-satellite is shown in Fig. 2. The dynamic model of the attitude of a micro-satellite is considered. The associated state vector is

$$\begin{array}{c} x = [x_1, x_2, x_3, x_4, x_5, x_6]^T \text{ or} \\ x = [\theta_1, \theta_2, \theta_3, \omega_1, \omega_2, \omega_3]^T \end{array} \tag{28}$$

where $\theta_1 = \phi$, $\theta_2 = \theta$, $\theta_3 = \psi$ to be the roll, pitch and yaw angles in the body-fixed reference frame, and $\omega_1 = \omega_x$, $\omega_2 = \omega_y$ and $\omega_3 = \omega_z$ to be the angular velocities of the satellite about the axes of the inertial reference frame. The control inputs vector is $u = [u_1, u_2, u_3]^T = [T_1, T_2, T_3]^T$ are torques which are provided by the satellite's actuation system. The satellite's dynamic model is written in the nonlinear affine-in-the-input state-space form

$$\dot{x} = f(x) + g(x)u + T_d \tag{29}$$

with $T_d$ to be the disturbances' vector. About the drift vector $f(x)$ and about the control inputs gain matrix $g(x)$ it holds that

$$f(x) = \begin{pmatrix} \frac{cos(x_3)x_5 - sin(x_3)x_6}{cos(x_2)} - \omega_0 \\ sin(x_3)x_5 + cos(x_3)x_6 \\ x_4 + \frac{sin(x_2)}{cos(x_2)}[sin(x_3)x_6 - cos(x_3)x_5] \\ \frac{I_2 - I_3}{I_1}[x_5 x_6 - 3\omega_0^2 \zeta_2 \zeta_3] \\ \frac{I_3 - I_1}{I_2}[x_6 x_4 - 3\omega_0^2 \zeta_3 \zeta_1] \\ \frac{I_1 - I_2}{I_3}[x_4 x_5 - 3\omega_0^2 \zeta_1 \zeta_2] \end{pmatrix} \quad g(x) = \begin{pmatrix} 0 & 0 & 0 \\ 0 & 0 & 0 \\ 0 & 0 & 0 \\ \frac{1}{I_1} & 0 & 0 \\ 0 & \frac{1}{I_2} & 0 \\ 0 & 0 & \frac{1}{I_3} \end{pmatrix} \tag{30}$$

where vector $\zeta$ is given by

$$\zeta = \begin{pmatrix} -sin(x_1)cos(x_2) \\ cos(x_1)sin(x_3) - sin(x_1)sin(x_2)cos(x_3) \\ cos(x_1)cos(x_3) - sin(x_1)sin(x_2)sin(x_3) \end{pmatrix} \tag{31}$$

The state-variables of the micro-satellite is now separated into two sub-vectors

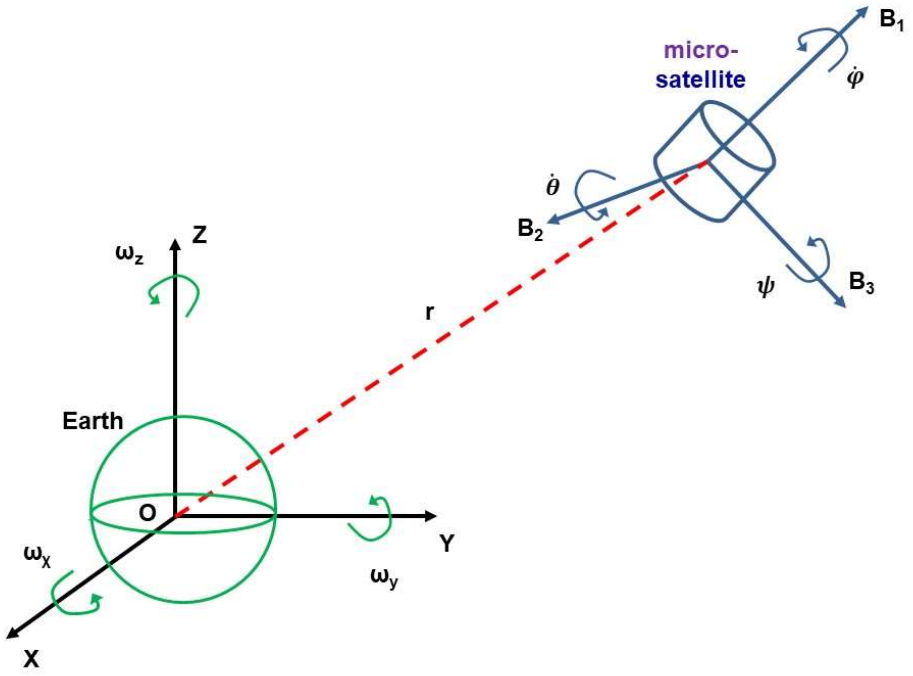


Figure 2: Diagram of the micro-satellite

$$\begin{aligned} x_a &= [x_1, x_2, x_3]^T \Rightarrow x_a = [\theta_1, \theta_2, \theta_3]^T \\ x_b &= [x_4, x_5, x_6]^T \Rightarrow x_a = [\omega_1, \omega_2, \omega_3]^T \end{aligned} \tag{32}$$

One also defines the following drift sub-vector and control inputs gain matrix for subsystem of the micro-satellite which us associated with the state sub-vector $x_a$

$$f_a(x) = \begin{pmatrix} -\omega_0 \\ 0 \\ 0 \end{pmatrix} \quad g_a(x) = \begin{pmatrix} 0 & \frac{cos(x_3)}{sin(x_2)} & -\frac{sin(x_3)}{sin(x_2)} \\ 0 & cos(x_3) & sin(x_3) \\ 1 & \frac{sin(x_2)sin(x_3)}{cos(x_2)} & -\frac{sin(x_2)cos(x_3)}{cos(x_2)} \end{pmatrix} \tag{33}$$

Additionally, one defines the following drift sub-vector and control inputs gain matrix for subsystem of the micro-satellite which us associated with the state sub-vector $x_b$

$$f_b(x) = \begin{pmatrix} \frac{I_2 - I_3}{I_1}[x_5 x_6 - 3\omega_0^2 \zeta_2 \zeta_3] \\ \frac{I_3 - I_1}{I_2}[x_6 x_4 - 3\omega_0^2 \zeta_3 \zeta_1] \\ \frac{I_1 - I_2}{I_3}[x_4 x_4 - 3\omega_0^2 \zeta_1 \zeta_2] \end{pmatrix} \quad g_b(x) = \begin{pmatrix} \frac{1}{I_1} & 0 & 0 \\ 0 & \frac{1}{I_2} & 0 \\ 0 & 0 & \frac{1}{I_3} \end{pmatrix} \tag{34}$$

Thus, the dynamics of the micro-satellite is decomposed into two-subsystems

$$\dot{x}_a = f_a(x) + g_a(x) x_b \tag{35}$$

$$\dot{x}_b = f_b(x) + g_b(x) u \tag{36}$$

It can be proven that the dynamic model of the micro-satellite as described in Eq. (35) and Eq. (36) is a differentially flat system with flat output $y = x_a$. Indeed, from Eq. (35) it holds that the drift vector

$f_a(x)$ has constant elements, while the control inputs gain matrix $g_a(x)$ contains elements that depend on the variables which constitute the flat outputs vector $x_a$. Thus, by solving Eq. (35) with respect to vector $x_b$ one obtains

$$x_b = g_a^{-1}(x)[\dot{x}_a - f_a(x)] \tag{37}$$

which signifies that $x_b$ is a differential function of the flat output of the micro-satellite $y = x_a$. Besides, in Eq. (36) vector $f_b(x)$ is a function of the flat outputs vector $y$ and matrix $g_b(x)$ is constant. Thus, by solving Eq. (36) with respect to the control inputs vector one obtains

$$u = g_b^{-1}(x)[\dot{x}_b - f_b(x)] \tag{38}$$

which signifies that the control inputs vector $u$ is also a differential function of the flat outputs of the system. The above come to confirm that the micro-satellite's vector is differentially flat. Next, it will be proven that the subsystems of Eq. (33) and Eq. (36) are independently flat sub-systems, and that the satellite's dynamics can be controlled in successive flatness-based control loops.

**Table Ib**

**Parameters of the satellite's attitude dynamic model**

| *Parameter* | *Definition* |
|---|---|
| $\theta_1$ | turn angle for rotation around axis $B_1$ of the satellite-fixed frame |
| $\theta_2$ | turn angle for rotation around axis $B_2$ of the satellite-fixed frame |
| $\theta_3$ | turn angle for rotation around axis $B_3$ of the satellite-fixed frame |
| $\omega_x$ | angular speed for rotation around axis Ox of the earth-fixed frame |
| $\omega_y$ | angular speed for rotation around axis Oy of the earth-fixed frame |
| $\omega_z$ | angular speed for rotation around axis Oz of the earth-fixed frame |
| $I_x, I_y, I_z$ | moments of inertia in rotation around the axes of earth-fixed frame |
| $\omega_0$ | orbital rate of the satellite |

## 5 Flatness-based control in successive loops for the micro-satellite's dynamics

First, it will be shown that each one of the subsystems of Eq. (35) and Eq. (36), if viewed independently, is a differentially flat subsystem. Indeed, Eq. (35) is a differentially flat subsystem with flat output $x_a$. From Eq. (35) one solves for $x_b$ which is now viewed as a virtual control input. It holds that

$$x_b = g_a^{-1}(x)[\dot{x}_a - f_a(x)] \tag{39}$$

Since the drift vector $f_a(x)$ has constant elements and the control inputs gain matrix $g_a(x)$ has elements that depend on the variables of the flat outputs vector $x_a$ it holds that $x_b$ is a differential function of the flat output $x_a$. Therefore, the subsystem of Eq. (35) is differentially flat.

Equivalently, in the subsystem of Eq. (35) the flat outputs vector is taken to be $x_b$, while $x_a$ is viewed as a coefficients vector. Thus, $f_b(x)$ is a function of the flat output $x_b$ and $g_b(x)$ has constant elements. Consequently, solving Eq. (36) for the control inputs vector $u$ givens

$$u = g_b^{-1}(x)[\dot{x}_b - f_b(x)] \tag{40}$$

which signifies that $u$ is a also a differential function of the flat outputs vector $x_b$. Consequently, the subsystem of Eq. (36) is also differentially flat.

The control of the subsystems of Eq. (35) and Eq. (36) can be carried out following the design process of controllers for input-output linearized differentially flat system. For the subsystem of Eq. (35) the setpoint is denoted as $x_a^d$ and the value of the virtual control input $x_b$ which stabilizes this subsystem is given by

$$x_b^* = g_a^{-1}(x)[\dot{x}_a^d - f_a(x) - K_1(x_a - x_a^d)] \tag{41}$$

Matrix $K_1 \in R^{3\times 3}$ is a diagonal matrix with its diagonal elements $k_{ii} > 0$ for $i = 1, 2, 3$. For the subsystem of Eq. (36) the control inputs vector $u$ is selected so as to ensure that $x_b$ will converge to the targeted vector $x_b^*$, which in turn makes the subsystem of Eq. (36) converge to the associated setpoint. Actually, the setpoint of the second subsystem is $x_b^d = x_b^*$ and the control input $u$ is given by

$$u = g_b^{-1}(x)[\dot{x}_b^d - f_b(x) - K_2(x_b - x_b^d)] \tag{42}$$

Matrix $K_2 \in R^{3\times 3}$ is a diagonal matrix, with its diagonal elements to satisfy $k_{ii} > 0$ for $i = 1, 2, 3$. By substituting Eq. (41) into Eq. (35), as well as by substituting Eq. (42) into Eq. (36) one obtains the dynamics of the closed-loop system

$$\begin{array}{c}(\dot{x}_a - \dot{x}_a^d) + K_1(x_a - x_a^d) = 0 \\ (\dot{x}_b - \dot{x}_b^d) + K_2(x_b - x_b^d) = 0\end{array} \tag{43}$$

Next, by defining the tracking error variables $e_a = x_a - x_a^d$ and $e_b = x_b - x_b^d$ the tracking error dynamics of the micro-satellite becomes

$$\begin{array}{c}\dot{e}_a + K_1 e_a = 0 \Rightarrow lim_{t\to\infty} e_a(t) = 0 \Rightarrow lim_{t\to\infty} x_a(t) = x_a^d(t) \\ \dot{e}_b + K_2 e_b = 0 \Rightarrow lim_{t\to\infty} e_b(t) = 0 \Rightarrow lim_{t\to\infty} x_b(t) = x_b^d(t)\end{array} \tag{44}$$

Consequently, all state variables of the micro-satellite's attitude dynamics converge to the associated setpoints or

$$lim_{t\to\infty} x_i(t) = x_i^d(t) \ \forall \ i = 1, 2, \cdots, 6 \tag{45}$$

The global stability properties of the micro-satellite's control loop can be also proven through Lyapunov stability analysis. The following Lyapunov function is defined

$$V = \tfrac{1}{2}[e_a^T e_a + e_b^T e_b] \tag{46}$$

By differentiating $V$ in time and with the use of Eq. (21) one obtains

$$\begin{array}{c}\dot{V} = e_a^T \dot{e}_a + e_b^T \dot{e}_b \Rightarrow \dot{V} = e_a^T(-K_1 e_a) + e_b^T(-K_2 e_b) \Rightarrow \\ \dot{V} = -e_a^T K_1 e_a - e_b^T K_2 e_b \Rightarrow \dot{V} < 0\end{array} \tag{47}$$

It holds that $\dot{V}$ is strictly negative $\forall e_a \neq 0$ and $\forall e_b \neq 0$. It becomes 0 only when $e_a = 0$ and $e_b = 0$. Therefore, the Lyapunov function of the system is strictly diminishing and finally converges to 0, no matter what the initial conditions of the micro-satellite's tracking error are. Thus, the control loop of the micro-satellite is globally asymptotically stable.

Once again, an explicit demonstration of the exponential stabilization that is achieved by flatness-based control in successive loops is given next. The Lyapunov function of the control loop is written as:

$$V = \tfrac{1}{2}[\textstyle\sum_{i=1}^{3} e_i^2 + \sum_{j=4}^{6} e_j^2] \tag{48}$$

where $e_i$ $i = 1, \cdots, 3$ are the tracking errors for the state variables of the satellite associated with rotation angles around the axes of the body-fixed frame and $e_j$ $j = 4, \cdots, 6$ are the tracking errors for the state variables of the satellite associated with angular velocities around the axes of the earth-fixed frame. Equivalently, the first-order time-derivative of the Lyapunov function is written as

$$\dot{V} = -[\textstyle\sum_{i=1}^{3} k_{1,i} e_i^2 + \sum_{j=4}^{6} k_{2,j-3} e_j^2] \tag{49}$$

where $k_{1,i} > 0$ $i = 1, \cdots, 3$ are the diagonal elements of gain matrix $K_1$ and $k_{2,j-3} > 0$ $j = 4, \cdots, 6$ are the diagonal elements of gain matrix $K_2$. By denoting the minimum of the above-noted elements of the feedback gain matrices as $k_{min}$, that is

$$k_{min} = min\{k_{1,i} : \ i = 1, \cdots, 3 \text{ and } k_{2,j-3} : \ j = 4, \cdots, 6\} \tag{50}$$

and using Eq. (49) one obtains that

$$\begin{array}{c} \dot{V} \leq -k_{min}[\sum_{i=1}^{3} e_i^2 + \sum_{j=4}^{6} e_j^2] \\ \Rightarrow \dot{V} \leq -2k_{min}V \Rightarrow \dot{V} + 2k_{min}V \leq 0 \end{array} \tag{51}$$

From Eq. (51) one can demonstrate the exponential convergence of the Lyapunov function $V$ to 0.

A diagram with the implementation stages of multi-loop flatness-based control method is given in Fig. 3. Once the state-space model of the system has been separated into chained subsystems which individually satisfy the differential flatness property, flatness-based control is implemented at each time-step through the following steps: (i) the state vector of the subsequent $(i+1)$-th subsystem becomes virtual control input to the preceding $i$-th subsystem, (ii) Equivalently, the virtual control input of the preceding $i$-th subsystem becomes setpoint for the subsequent $(i+1)$-th subsystem, (iii) the value of the virtual control input for each subsystem is computed by inverting the dynamics of this subsystem and by selecting feedback gains which allow for eliminating the associated local tracking error, (iv) the real control input is computed from the last subsystem by inverting again the dynamics of this subsystem (v) the real control input makes implicitly use of the virtual control inputs of all preceding subsystems. Its stabilizing effects appear by tracing the subsystems of the state-space model backwards from the last to the first one.

## 6 Simulation tests

### 6.1 Outline of the simulation results

The aim of the simulation tests has been to evaluate the tracking performance of the 6-DOF autonomous octocopter of the 3-DOF micro-satellite. In particular: (1) Fig. 4 to Fig. 11 present tracking of 4 different setpoints by the state variables of the 6-DOF autonomous octocopter. In each test case there are 2 subfigures depicting the variations of the 12 state variables of this drone and 1 subfigure depicting the variations of the 4 control inputs of this unmanned aerial vehicle. Moreover, there is one subfigure demonstrating in 3D plots the tracking of helicoidal reference trajectories by this drone in the cartesian space. Besides Tables IIa to IIIa analyze the tracking performance of the flatness-based control method in successive loops when considering an exactly known model of the 6-DOF octocopter and when considering a model of this drone which is subject to perturbations. (2) Fig. 12 to Fig 19 present tracking of 4 different setpoints by the state variables of the 3-DOF micro-satellite. In each test case there are 2 subfigures depicting the variations of the 6 state variables of the micro-satellite, 1 subfigure depicting the tracking error of the rotation angles around the axes of the satellite's body-fixed frame and 1 subfigure plotting the variations of the 3 control inputs of the satellite. Tables IIb to IIIb analyze the tracking performance in the orientation of the satellite under flatness-based control in successive loops and by considering first an exactly known dynamic model of the micro-satellite and next a dynamic model that is subject to disturbances.

### 6.2 Control of the 6-DOF autonomous octocopter

Results about the tracking accuracy and the speed of convergence to setpoints of the successive-loops flatness-based control method, in the case of the 6-DOF autonomous octocopter, are shown in Fig. 4 to Fig. 11. Indicative values about the parameters of the dynamic model of the 6-DOF autonomous aircraft have been as follows: $m = 2kg$, $I_{rotor} = 1.3kg \cdot m^2$, $L = 1.5m$, $g = 10m/sec^2$, $K_{ft,x} = 0.1$, $K_{ft,y} = 0.1$,

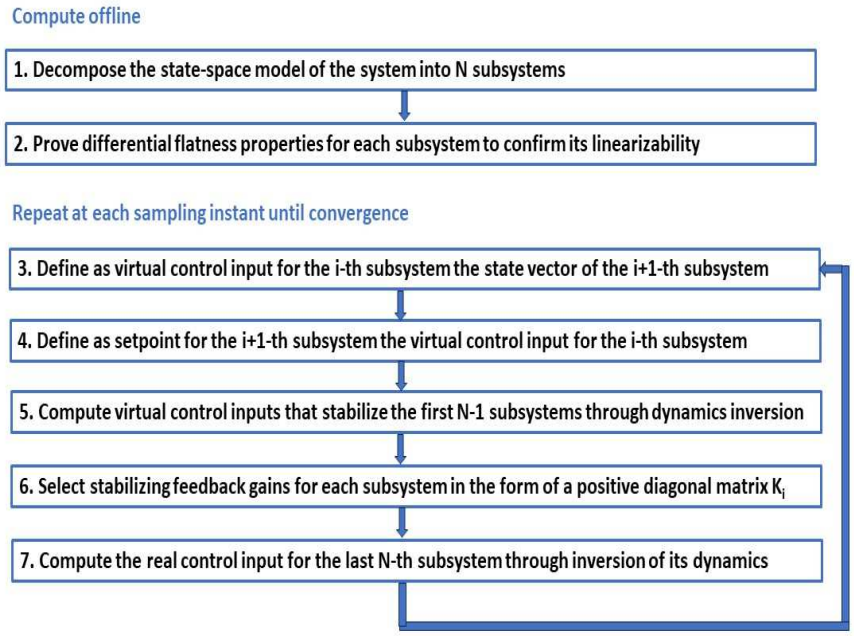


Figure 3: Diagram with the implementation stages of multi-loop flatness-based control

$K_{ft,z} = 0.1$, $K_{fa,x} = 0.2$, $K_{fa,y} = 0.2$, $K_{fa,z} = 0.2$, $I_x = 1.6kg \cdot m^2$, $I_y = 1.6kg \cdot m^2$, $I_z = 1.6kg \cdot m^2$. Gain matrix $K_1$ is diagonal with the elements on its diagonal to be given the value $k_{1,ii} = 0.3$ for $i = 1, \cdots, 6$. Gain matrix $K_2$ is also diagonal with the elements on its diagonal to be given the value $k_{2,ii} = 0.8$ for $i = 1, \cdots, 6$.

To elaborate on flatness-based control in successive loops for the unmanned octocopter the following Tables are given (i) Table IIa providing results about the accuracy of tracking of setpoints by the state variables of the unmanned octocopter under an exact dynamic model, (ii) Table IIIa providing results about the accuracy of tracking of setpoints by the state variables of the unmanned octocopter under a model that is subject to disturbances (for instance change $\Delta\alpha\%$ in the mass $m$ of the UAV's dynamic model).

**Table IIa**

**Tracking RMSE $\times 10^{-3}$ for the 6-DOF octocopter UAV in the disturbance-free case**

| | $RMSE_{x_1}$ | $RMSE_{x_2}$ | $RMSE_{x_3}$ | $RMSE_{x_4}$ | $RMSE_{x_5}$ | $RMSE_{x_6}$ | $RMSE_{x_7}$ | $RMSE_{x_9}$ | $RMSE_{x_{11}}$ |
|---|---|---|---|---|---|---|---|---|---|
| $\text{test}_1$ | 0.1216 | 0.0359 | 0.1360 | 0.0759 | 0.0001 | 0.0001 | 0.0001 | 0.0001 | 0.0001 |
| $\text{test}_2$ | 0.5401 | 0.3312 | 0.7210 | 0.4411 | 0.0001 | 0.0001 | 0.0001 | 0.0001 | 0.0001 |
| $\text{test}_3$ | 0.7749 | 0.5180 | 0.6207 | 0.4140 | 0.0001 | 0.0001 | 0.0001 | 0.0001 | 0.0001 |
| $\text{test}_4$ | 0.7210 | 0.4411 | 0.9002 | 0.5521 | 0.0001 | 0.0001 | 0.0001 | 0.0001 | 0.0001 |

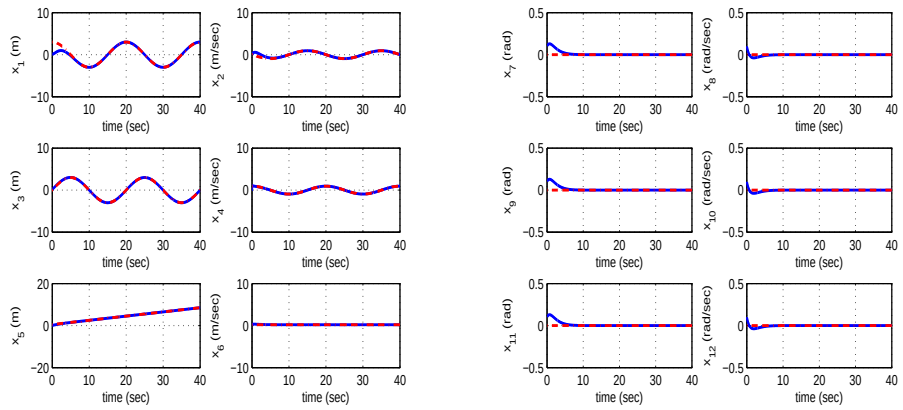


**(a)** **(b)**

Figure 4: Tracking of trajectory 1 by the 6-DOF autonomous octocopter (a) convergence of state variables $x_1$ to $x_6$ to their reference setpoints (red line: setpoint, blue line: real value), (b) convergence of state variables $x_7$ to $x_{12}$ to their reference setpoints (red line: setpoint, blue line: real value)

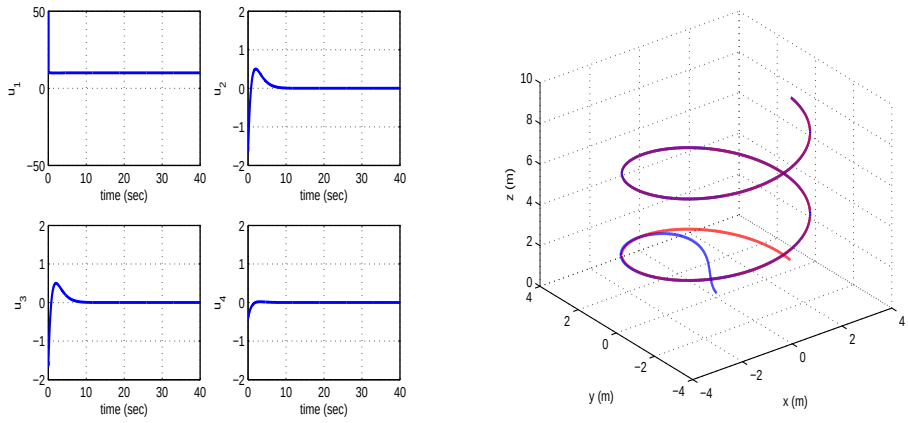


**(a)** **(b)**

Figure 5: Tracking of trajectory 1 by the 6-DOF autonomous octocopter (a) variation of the control inputs $u_1$ to $u_4$ (blue line), (b) tracking of the reference flight path by the UAV in the $xyz$ cartesian space

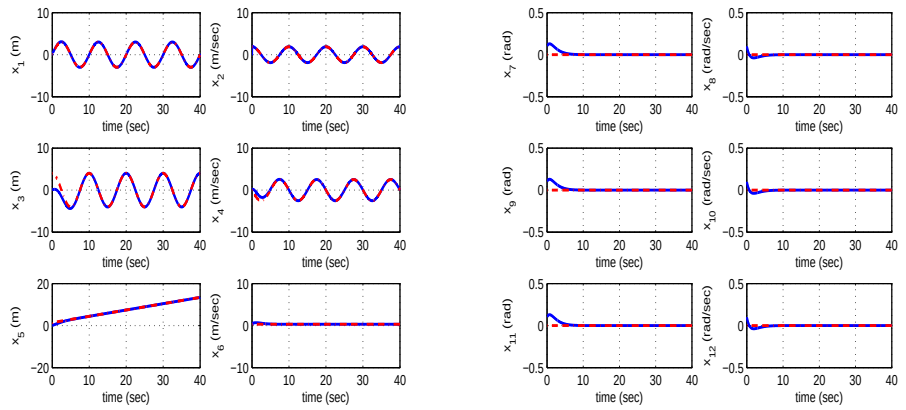


**(a)** **(b)**

Figure 6: Tracking of trajectory 2 by the 6-DOF autonomous octocopter (a) convergence of state variables $x_1$ to $x_6$ to their reference setpoints (red line: setpoint, blue line: real value), (b) convergence of state variables $x_7$ to $x_{12}$ to their reference setpoints (red line: setpoint, blue line: real value)

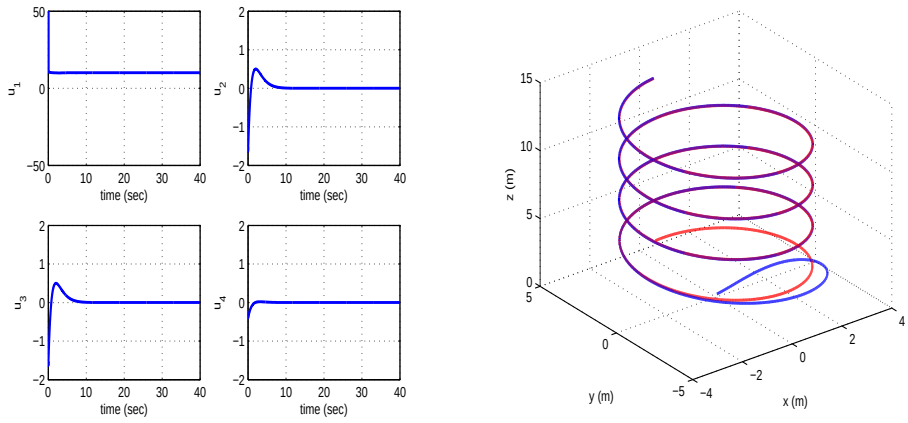


**(a)** **(b)**

Figure 7: Tracking of trajectory 2 by the 6-DOF autonomous octocopter (a) variation of the control inputs $u_1$ to $u_4$ (blue line), (b) tracking of the reference flight path by the UAV in the $xyz$ cartesian space

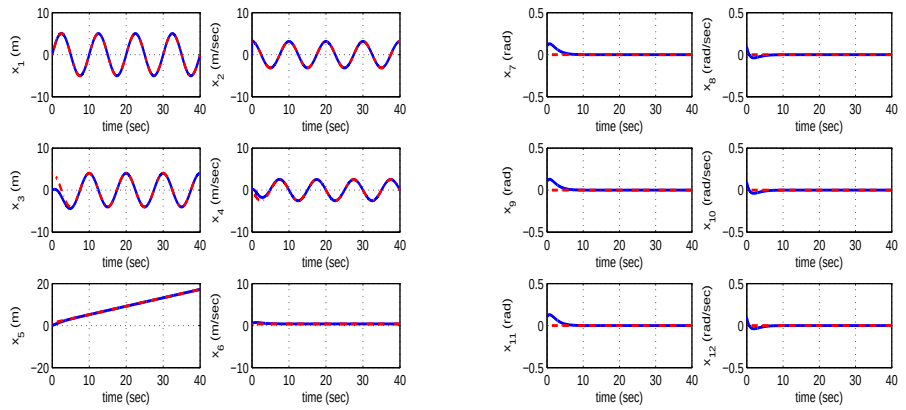


**(a)** **(b)**

Figure 8: Tracking of trajectory 3 by the 6-DOF autonomous octocopter (a) convergence of state variables $x_1$ to $x_6$ to their reference setpoints (red line: setpoint, blue line: real value), (b) convergence of state variables $x_7$ to $x_{12}$ to their reference setpoints (red line: setpoint, blue line: real value)

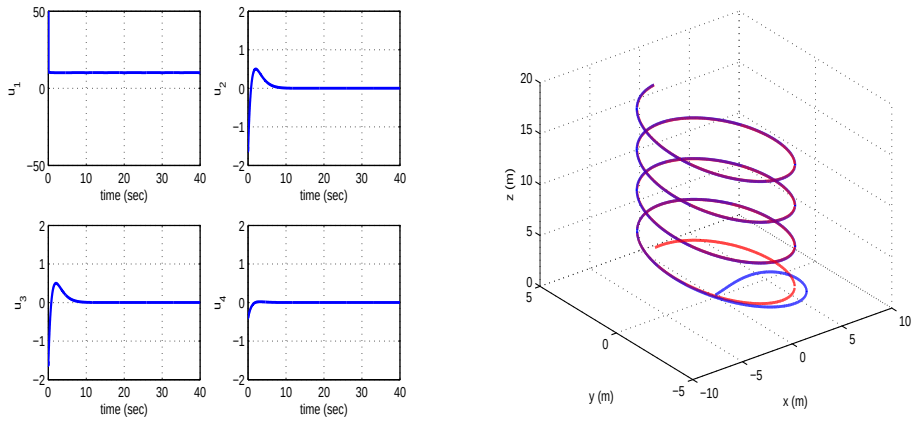


**(a)** **(b)**

Figure 9: Tracking of trajectory 3 by the 6-DOF autonomous octocopter (a) variation of the control inputs $u_1$ to $u_4$ (blue line), (b) tracking of the reference flight path by the UAV in the $xyz$ cartesian space

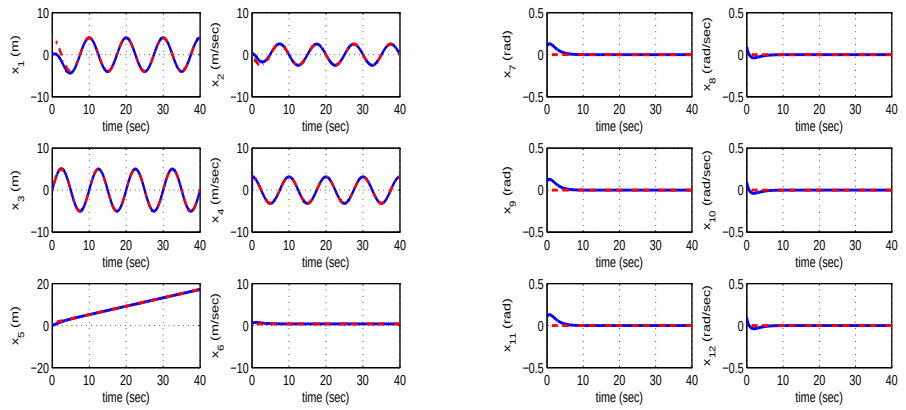


**(a)** **(b)**

Figure 10: Tracking of trajectory 4 by the 6-DOF autonomous octocopter (a) convergence of state variables $x_1$ to $x_6$ to their reference setpoints (red line: setpoint, blue line: real value), (b) convergence of state variables $x_7$ to $x_{12}$ to their reference setpoints (red line: setpoint, blue line: real value)

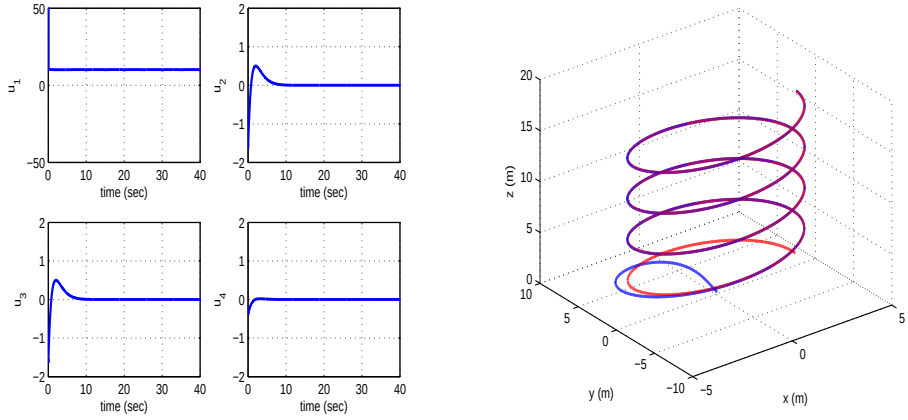


**(a)** **(b)**

Figure 11: Tracking of trajectory 4 by the 6-DOF autonomous octocopter (a) variation of the control inputs $u_1$ to $u_4$ (blue line), (b) tracking of the reference flight path by the UAV in the $xyz$ cartesian space

| Table IIIa | | | | | | | | | |
|---|---|---|---|---|---|---|---|---|---|
| **Tracking RMSE $\times 10^{-3}$ for the 6-DOF octocopter UAV in the case of disturbances** | | | | | | | | | |
| $\Delta a\%$ | $RMSE_{x_1}$ | $RMSE_{x_2}$ | $RMSE_{x_3}$ | $RMSE_{x_4}$ | $RMSE_{x_5}$ | $RMSE_{x_6}$ | $RMSE_{x_7}$ | $RMSE_{x_9}$ | $RMSE_{x_{11}}$ |
| 0% | 0.1216 | 0.0359 | 0.1360 | 0.0759 | 0.0001 | 0.0001 | 0.0001 | 0.0001 | 0.0001 |
| 10% | 0.1434 | 0.0010 | 0.1470 | 0.0022 | 0.0636 | 0.0001 | 0.0001 | 0.0001 | 0.0001 |
| 20% | 0.3305 | 0.0279 | 0.2070 | 0.0591 | 0.1166 | 0.0001 | 0.0001 | 0.0001 | 0.0001 |
| 30% | 0.4933 | 0.0524 | 0.2719 | 0.1108 | 0.1614 | 0.0001 | 0.0001 | 0.0001 | 0.0001 |
| 40% | 0.6334 | 0.0773 | 0.3318 | 0.1551 | 0.1998 | 0.0001 | 0.0001 | 0.0001 | 0.0001 |
| 50% | 0.7549 | 0.0914 | 0.3853 | 0.1934 | 0.2332 | 0.0001 | 0.0001 | 0.0001 | 0.0001 |
| 60% | 0.8612 | 0.1072 | 0.4329 | 0.2269 | 0.2623 | 0.0001 | 0.0001 | 0.0001 | 0.0001 |

### 6.3 Control of the 3-DOF micro-satellite's attitude dynamics

Results about the tracking accuracy and the speed of convergence to setpoints of the successive-loops flatness-based control method, in the case of the 3-DOF micro-satellite's attitude dynamics, are shown in Fig. 12 to Fig. 19. Indicative values about the parameters of the dynamic model of the 3-DOF microsatellite have been as follows: $I_1 = 28.4kg \cdot m^2$, $I_2 = 18.4kg \cdot m^2$, $I_3 = 16.8kg \cdot m^2$ while the orbital rate was $\omega_0 = 0.0011$. Gain matrix $K_1$ is diagonal with the elements on its diagonal to be given the value $k_{1,ii} = 0.3$ for $i = 1, \cdots, 3$. Gain matrix $K_2$ is also diagonal with the elements on its diagonal to be given the value $k_{2,ii} = 0.8$ for $i = 1, \cdots, 3$. Regarding the setpoints which have been used in the 4 test cases about the micro-satellite's attitude control the following can be noted:

Setpoints 1 to 4 describe piece-wise constant desirable values $\theta_1^d$, $\theta_2^d$, $\theta_3^d$ for the first three state variables of the micro-satellite's attitude dynamic model, that is for the orientation angles in the body-fixed frame. The setpoints for the angular velocities $\omega_1^d$, $\omega_2^d$, $\omega_3^d$ of the satellite in the inertial reference frame are computed from the differential relations which connect the angular speed state variables with the turn angle flat outputs of the system. As expected, the setpoints $\omega_1^d$, $\omega_2^d$, $\omega_3^d$ converge very fast to the zero value. This signifies that upon convergence of the satellite's state variables to the associated setpoints the satellite gets stabilized at the desirable orientation angles and stops rotating.

It can be noticed again, that under this control scheme one achieves fast and precise tracking of reference setpoints for all state variables of the dynamic model of the attitude of the micro-satellite. It is noteworthy, that through the stages of this method one solves also the setpoints definition problem for all state variables of the micro-satellite. Actually, the selection of setpoints for state variables $x_1$, $x_2$ and $x_2$ is unconstrained. On the other side by defining state variables $x_4$, $x_5$, $x_9$ and $x_6$ as virtual control inputs for the subsystem of $x_1$, $x_2$ and $x_3$ one can find the setpoints for $x_4$ to $x_6$ as functions of the setpoints for $x_1$ to $x_3$. The speed of convergence of the state variables of the micro-satellite's attitude dynamics under flatness-based control implemented in successive loops is determined by the selection of values for the diagonal gain matrices $K_1$, $K_2$.

To elaborate on flatness-based control in successive loops for the micro-satellite the following Tables are given (i) Table IIb providing results about the accuracy of tracking of setpoints by the state variables of the micro-satellite under an exact dynamic model, (ii) Table IIIb providing results about the accuracy of tracking of setpoints by the state variables of the micro-satellite under a model that is subject to disturbances (for instance change $\Delta\alpha\%$ in the orbital rate variable $\omega_0$ of the satellite's dynamic model).

| Table IIb | | | | | | |
|---|---|---|---|---|---|---|
| **Tracking RMSE $\times 10^{-4}$ for the 3-DOF micro-satellite in the disturbance-free case** | | | | | | |
| | $RMSE_{x_1}$ | $RMSE_{x_2}$ | $RMSE_{x_3}$ | $RMSE_{x_4}$ | $RMSE_{x_5}$ | $RMSE_{x_6}$ |
| $\text{test}_1$ | 0.0210 | 0.0146 | 0.0404 | 0.0001 | 0.0001 | 0.0001 |
| $\text{test}_2$ | 0.0298 | 0.0073 | 0.1485 | 0.0001 | 0.0001 | 0.0001 |
| $\text{test}_3$ | 0.0316 | 0.0155 | 0.1602 | 0.0003 | 0.0001 | 0.0001 |
| $\text{test}_4$ | 0.0418 | 0.0777 | 0.0056 | 0.0036 | 0.0003 | 0.0002 |

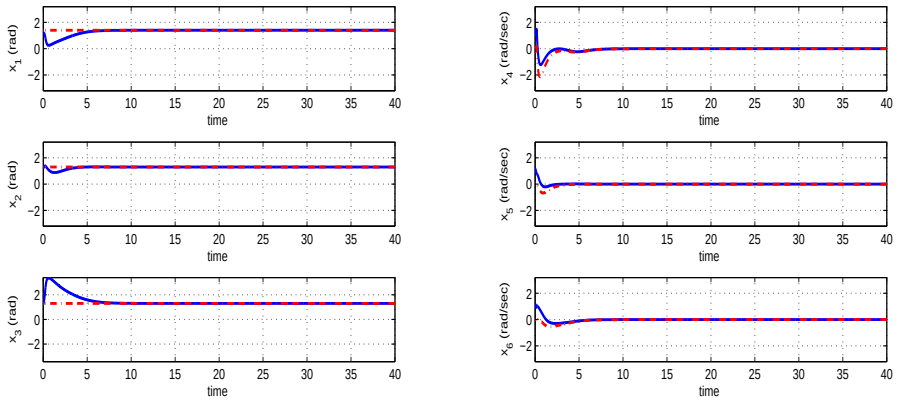


**(a)** **(b)**

Figure 12: Attitude control for the 3-DOF micro-satellite when tracking setpoint 1 (a) convergence of state variables $x_1$ to $x_3$ to their reference setpoints (red line: setpoint, blue line: real value), (b) convergence of state variables $x_4$ to $x_6$ to their reference setpoints (red line: setpoint, blue line: real value)

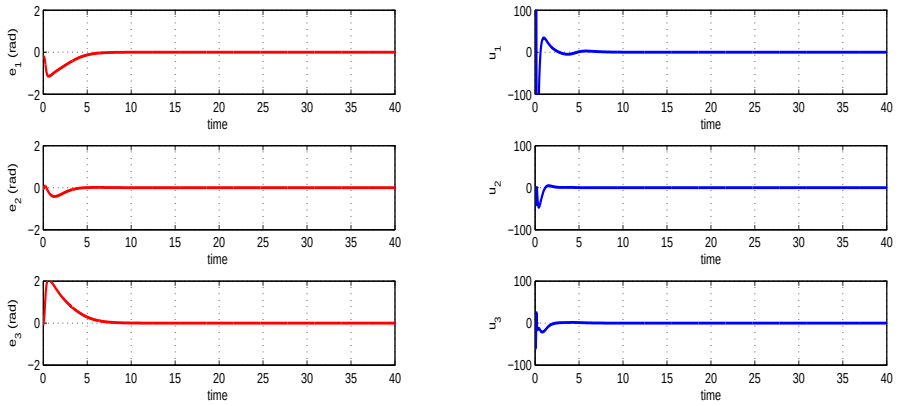


**(a)** **(b)**

Figure 13: Attitude control for the 3-DOF micro-satellite when tracking setpoint 1 (a) tracking error of state variables $x_1$ to $x_3$, that is the orientation angles in the body-fiex frame (red line), (b) variation of the control inputs $u_1$ to $u_3$ (blue line)

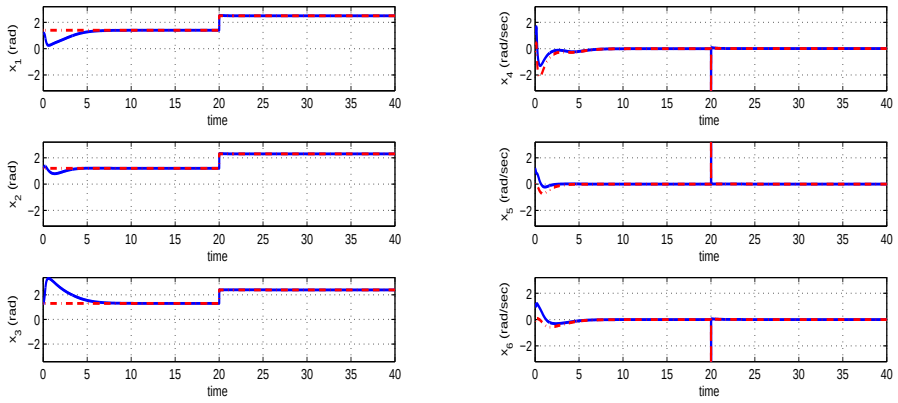


**(a)** **(b)**

Figure 14: Attitude control for the 3-DOF micro-satellite when tracking setpoint 2 (a) convergence of state variables $x_1$ to $x_3$ to their reference setpoints (red line: setpoint, blue line: real value), (b) convergence of state variables $x_4$ to $x_6$ to their reference setpoints (red line: setpoint, blue line: real value)

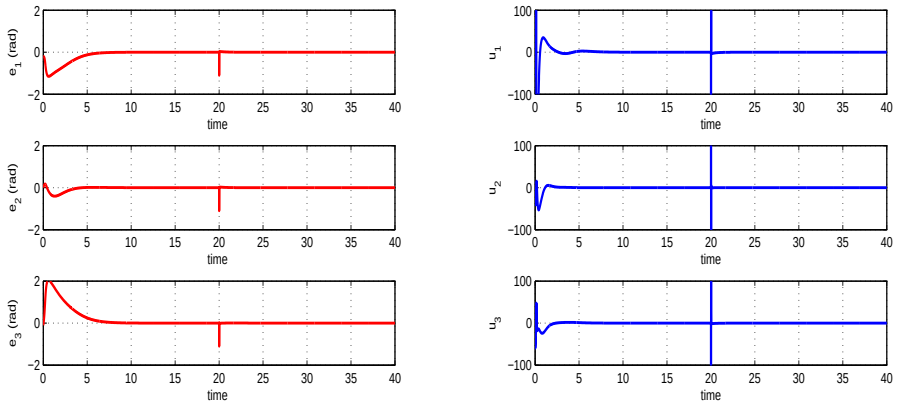


**(a)** **(b)**

Figure 15: Attitude control for the 3-DOF micro-satellite when tracking setpoint 2 (a) tracking error of state variables $x_1$ to $x_3$, that is the orientation angles in the body-fiex frame (red line), (b) variation of the control inputs $u_1$ to $u_3$ (blue line)

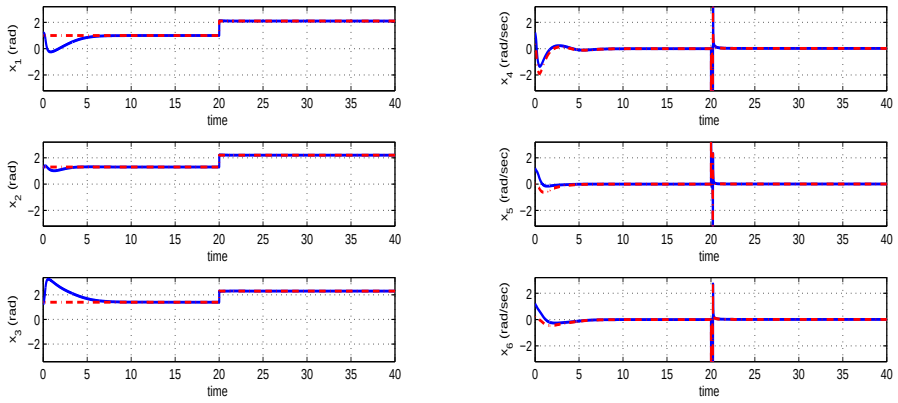


**(a)** **(b)**

Figure 16: Attitude control for the 3-DOF micro-satellite when tracking setpoint 3 (a) convergence of state variables $x_1$ to $x_3$ to their reference setpoints (red line: setpoint, blue line: real value), (b) convergence of state variables $x_4$ to $x_6$ to their reference setpoints (red line: setpoint, blue line: real value)

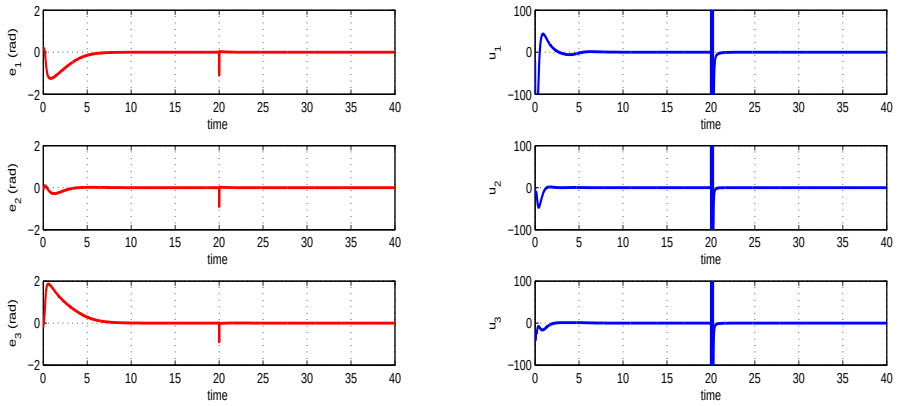


**(a)** **(b)**

Figure 17: Attitude control for the 3-DOF micro-satellite when tracking setpoint 3 (a) tracking error of state variables $x_1$ to $x_3$, that is the orientation angles in the body-fiex frame (red line), (b) variation of the control inputs $u_1$ to $u_3$ (blue line)

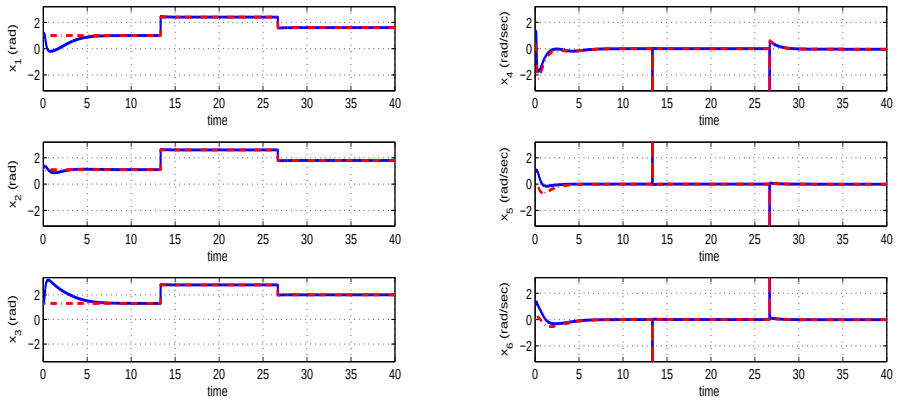


**(a)** **(b)**

Figure 18: Attitude control for the 3-DOF micro-satellite when tracking setpoint 4 (a) convergence of state variables $x_1$ to $x_3$ to their reference setpoints (red line: setpoint, blue line: real value), (b) convergence of state variables $x_4$ to $x_6$ to their reference setpoints (red line: setpoint, blue line: real value)

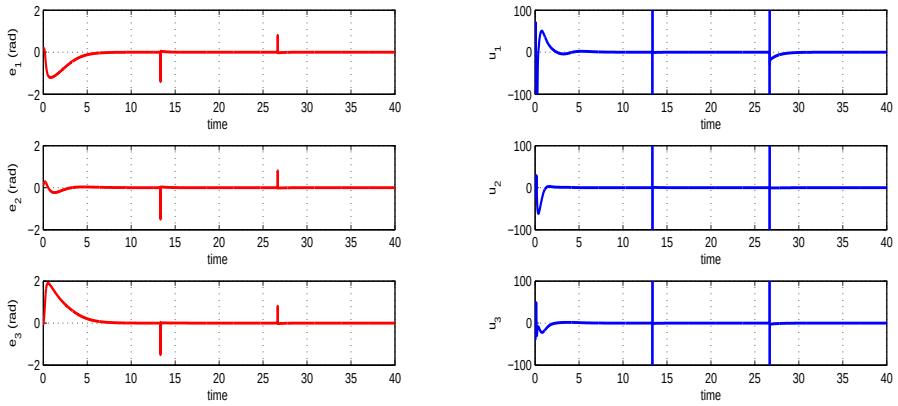


**(a)** **(b)**

Figure 19: Attitude control for the 3-DOF micro-satellite when tracking setpoint 4 (a) tracking error of state variables $x_1$ to $x_3$, that is the orientation angles in the body-fiex frame (red line), (b) variation of the control inputs $u_1$ to $u_3$ (blue line)

| Table IIIb | | | | | | |
|---|---|---|---|---|---|---|
| **Tracking RMSE $\times 10^{-4}$ for the 3-DOF micro-satellite in the case of disturbances** | | | | | | |
| $\Delta a\%$ | $RMSE_{x_1}$ | $RMSE_{x_2}$ | $RMSE_{x_3}$ | $RMSE_{x_4}$ | $RMSE_{x_5}$ | $RMSE_{x_6}$ |
| 0% | 0.0298 | 0.0073 | 0.1485 | 0.0001 | 0.0001 | 0.0001 |
| 10% | 0.0299 | 0.0073 | 0.1486 | 0.0001 | 0.0001 | 0.0001 |
| 20% | 0.0299 | 0.0073 | 0.1487 | 0.0001 | 0.0001 | 0.0001 |
| 30% | 0.0300 | 0.0074 | 0.1489 | 0.0001 | 0.0001 | 0.0001 |
| 40% | 0.0300 | 0.0074 | 0.1490 | 0.0001 | 0.0001 | 0.0001 |
| 50% | 0.0301 | 0.0074 | 0.1492 | 0.0001 | 0.0002 | 0.0001 |
| 60% | 0.0302 | 0.0074 | 0.1494 | 0.0001 | 0.0003 | 0.0002 |

One can see the advantages of the proposed flatness-based control methods in successive loops in comparison to global linearization-based control methods, which require the transformation of the system's dynamics in the input-output linearized form and in the associated canonical Brunovsky form through changes of state variables (diffeomorphisms) and complicated transformations of the system's state-space model. The latter is the case of Lie-algebra-based control and of flatness-based control through input-output linearization. In Lie algebra-based control to arrive at an input-to-state or input-output linearized description of the system, successive computations of Lie derivatives have to be performed based on the linearizing outputs of the system and on the drift vector and control input gains vectors of the initial nonlinear model. Obviously, elaborated computations are needed while the resulting linearized form usually consists of elongated mathematical formulas which incur additional complexity to the system's dynamics. For the linearized state-space model one finds a stabilizing feedback control in a phenomenally easy manner and by applying the eigenvalues assignment technique. However, to compute the control inputs which should be applied to the initial nonlinear state-space model of the system, once again complicated inverse transformations have to be applied which may also come against singularity (matrices non-invertibility) issues. In contrast to the above, the proposed nonlinear optimal control method achieves global stability and setpoints tracking for the controlled system by generating control inputs which are applied directly on the initial nonlinear model of the system and without the involvement of any forward or backwards transformations.

## 7 Conclusions

In the new flatness-based control approach which is implemented in successive loops the state-space model of the nonlinear system is decomposed into subsystems, which satisfy differential flatness properties. For each subsystem of the state-space model a virtual control input is computed, capable of inverting the subsystem's dynamics and of eliminating the subsystem's tracking error. The control input that is actually applied to the nonlinear system is found from the last row of the state-space description. This control input incorporates in a recursive manner all virtual control inputs which were computed for the individual subsystems associated with the initial state-space equation. The control input that should be applied to the nonlinear system so as to assure that all its state vector elements will converge to the desirable setpoints, is obtained at each iteration of the control algorithm, by tracing the subsystems of the state-space model backwards.

The proposed method of flatness-based control in successive loops is applied to the control problem of the multivariable and nonlinear dynamics of unmanned aerial vehicles and micro-satellites. The state-space model of (i) unmanned aerial vehicles and (ii) micro-satellites is separated into two subsystems, which are connected between them in cascading loops. Each one of these subsystems can be viewed independently as a differentially flat system and control about it can be performed with inversion of its dynamics as in the case of input-output linearized flat systems. The state variables of the second subsystem become virtual control inputs for the first subsystem. In turn exogenous control inputs are applied to the first subsystem. The whole control method is implemented in two successive loops and its global stability properties are

also proven through Lyapunov stability analysis. The following application examples have confirmed the method's fine performance: (a) control of a 6-DOF autonomous octocopter, (ii) control of a 3-DOF dynamic model of the attitude of a micro-satellite. The control scheme is sufficiently robust to parametric changes. The new control method achieved fast and accurate tracking of reference setpoints under moderate variations of the control inputs.

## References


[1] G. Rigatos, Nonlinear control and filtering using differential flatnesss theory approaches: Applications to electromechanical systems, Springer, 2016

[2] G. Rigatos and K. Busawon, Robotic manipulators and vehicles: Control, estimation and filtering, Springer, 2018

[3] G. Rigatos, M. Abbaszadeh, P. Siano, Control and estimation of dynamical nonlinear and partial differential equation systems: Theory and Applications, IET Publications, 2022

[4] J.Levine, Analysis and Control of Nonlinear Systems: A flatness-based approach, Springer 2009.

[5] M. Fliess and H. Mounier, Tracking control and $\pi$-freeness of infinite dimensional linear systems, In: G. Picci and D.S. Gilliam Eds.,Dynamical Systems, Control, Coding and Computer Vision, vol. 258, pp. 41-68, *Birkhaüser*, 1999.

[6] J. Villagra, B. d'Andrea-Novel, H. Mounier and M. Pengov, Flatness-based vehicle steering control strategy with SDRE feedback gains tuned via a sensitivity approach, IEEE Transactions on Control Systems Technology, vol. 15, pp. 554- 565, 2007.

[7] S. Bououden, D. Boutat, G. Zheng, J.P. Barbot and F. Kratz, A triangular canonical form for a class of 0-flat nonlinear systems, International Journal of Control, Taylor and Francis, vol. 84, no. 2, pp. 261-269, 2011.

[8] L. Menhour, B. d'Andre'a-Novel, M. Fliess and H. Mounier, Coupled nonlinear vehicle control: Flatness-based setting with algebraic estimation techniques, Control Engineering Practice, Elsevier, vol. 22, pp. 135–146, 2014

[9] F. Nicolaum W. Respondek and J.P. Barbot, How to minimally modify a dynamical system when constructing flat inputs, Internattional Journal of Robust and Nonlinear Control, J. Wiley, 2022.

[10] C. Letelier nd J.P. Barbot, Optimal flatness placement of sensors and actuators for controlling chaotic systemsm Chaos, AIP Publications, vol. 31, no. 10, article No 103114, 2021.

[11] H. Sira-Ramirez and S. Agrawal, Differentially Flat Systems, Marcel Dekker, New York, 2004.

[12] J. Lévine, On necessary and sufficient conditions for differential flatness, Applicable Algebra in Engineering, Communications and Computing, Springer, vol. 22, no. 1, pp. 47-90, 2011.

[13] F. Nicolau, W. Respondek and J.P. Barbot, Construction of flat inputs for mechanical systems, 7th IFAC Workshop on Lagrangian and Hamiltonian methods for nonlinear control, Berlin, Germany, OCt. 2021

[14] J.O. Limaverde Filho, E.C.R. Fortaleza and M.C.M. Campos, A derivative-free nonlinear Kalman Filtering approach using flat inputs, International Journal of Control, Taylor and Francis 2021.

[15] J.P. Barbot, M. Fliess and T. Floquet, An algebraic framework for the design of nonlinear observers with uknown inputs, IEEE CDC 2007, IEEE 46th Intl. Conference on Decision and Control, New Orleans, USA, Dec. 2007

[16] H. Khalil, Nonlinear Systems, Prentice Hall, 1996

[17] G.G. Rigatos and S.G. Tzafestas, Extended Kalman Filtering for Fuzzy Modelling and Multi-Sensor Fusion, Mathematical and Computer Modelling of Dynamical Systems, Taylor & Francis), vol. 13, pp. 251-266, 2007.

[18] M. Basseville and I. Nikiforov, Detection of abrupt changes: Theory and Applications, *Prentice-Hall*, 1993.

[19] G. Rigatos and Q. Zhang, Fuzzy model validation using the local statistical approach, Fuzzy Sets and Systems, Elsevier, vol. 60, no. 7, pp. 882-904,2009.

[20] G. Rigatos, P. Siano and N. Zervos, A new concept of flatness-based control of nonlinear dynamical systems, IEEE INDIN 2015, 13th IEEE Intl. Conf. on Industrial Informatics, Cambridge, UK, July 2015

[21] G. Rigatos, P. Siano, S Ademi and P. Wira, Flatness-based control of DC-DC converters implemented in successive loops, Electric Power Components and Systems, Taylor and Francis, vol. 46, no. 6, pp. 673-687, 2018.

[22] G. Rigatos, Flatness-based embedded control in successive loops for spark ignited engines, Journal of Physics, IOP Publications, Conference Series No 659, 012019, IFAC ACD 2015, Proc. of the 12th European Workshop on Advanced Control and Diagnosis.

[23] G. Rigatos and A. Melkikh, Flatness-based control in successive loops for stabilization of heart's electrical activity, In Proc. ICNAAM 2016, AIP Conf. Proceedings No 1790 060004, Intl. Conf. on Numerical Analysis and Applied Mathematics, 2016

[24] G. Rigatos, P. Wira, M. Abbaszadeh and J. Pomares, Flatness-based control in successive loops for industrial and mobile robots, IEEE IECON 2022, IEEE 48th Annual Conference of the Industrial Electronics Society, Brussels, Belgium, Oct. 2022

[25] G. Rigatos, P. Wira, M. Abbaszadeh and P. Siano, A nonlinear optimal control approach for the Lotka-Volterra dynamical system, IEEE IECON 2022, IEEE 48th Annual Conference of the Industrial Electronics Society, Brussels, Belgium, Oct. 2022

[26] G. Rigatos and P. Siano, Flatness-based control in successive loops for Business Cycles of Finance Agents, Journal of Intelligent Industrial Systems, Springer, vol. 3, pp. 77-89, 2017

[27] H. Alwi and C. Edwards, Sliding-mode fault tolerant control of an octorotor using linear parameter varying-based schemes, IET Control Theory and Applications, vol. 9, no. 4, pp. 618-636, 2015

[28] F. Bauer, C.H. Hackl, K.M. Smedley and R.M. Kennel, Multicopter with series connected propeler drives, IEEE Transactions on Control Systems Technology, vol. 26, no. 2, pp. 563-574, 2016

[29] S. Zeglache, H. Mekki, A. Boufouerra and A. Djerioui, Actuator fault tolerant control using adaptive RBFNN fuzzy sliding mode controller for co-axial octorotor UAV, ISA Transactions, Elsevier, 2019

[30] Y. Bouzid, H. Siguerdidjane and Y. Bestaoui, Hirearchical autopilot design based on immersion and invariance and nonlinear internal model tracking controllers for autonomous system, 4th IFAC International Conference on Intelligent Control and Automation Sciences (ICONS 2016), Jun 2016, Reims, France.

[31] A. Marks, J.F. Whidborne and J. Yamamoto, Control allocation for fault tolerant control of a VTOL octorotor, IEEE UKACC 2012, IEEE UK Automatic Control Conference, Cardiff, UK, Sep. 2012

[32] A.R. Merheb, H. Noura and F. Bateman, Active fault tolerant control of Octorotor UAV using dynamic control allocation, IEEE ICIUS 2014, The 2014 International Conference on Intelligent Unmanned systems, Montreal, Canada, 2014

[33] H. Alwi and C. Edwards, Fault tolerant control of octorotor using sliding-mode control allocation, Proc. EuroGNC 2013, 2nd CEAS Specialist Conference on Guidance, Navigation and Control, Delft, The Netherlands, April 2013.

[34] H. Alwi, M.T. Hamayan and C. Edwards, An integral sliding-mode fault tolerant control scheme for an octorotor using fixed control allocation, 13th IEEE Workshop on Variable Structure Systems, IEEE VSS 2014, Nantes, France, July 2014

[35] H. Saied, B. Lussier, I. Fantoni H. Shraim and C. Francis, Passive fault-tolerant control of an octorotor using super-twisting algorithm: Theory and experiments, IEEE SysTol 2016, IEEE 3rd Conf. on Control and Fault-tolerant Systems, Barcelona, Spain, Sep. 2016

[36] T. Chevet, M. Makarov, C. Stoica-Maniu, I. Hinostroza and P. Tarascon, State estimation of an octorotor with unknown inputs: applications to radar imaging, IEEE ICSTCC 2017, IEEE 21st Intl. Conf on Systems Theory, Control and Computing, Romania, 2017

[37] J.C. Salazar, A. Sanjuan, F. Nejjari and R. Sarrate, Health-aware control of an octorotor UAV system based on actuator reliability, IEEE CoDIT 2017, 2017 4th International Conference on Control, Decision and Information Technologies, April 2017, Barcelona, Spain.

[38] B. Wang, Y. Zhang, J.C. Ponsart and D. Theilliol, Fault-tolerant adaptive control allocation for unmanned multirotor helicopters, 20th IFAC World Congress, Toulouse, France, July 2017

[39] Y. Bouzid, H. Siguerdidjane and Y. Bestaoui, Improved 3D trajectory tracking by nonlinear internal-model-feedback linearization control strategy for autonomous systems, Part of special issue: 6th IFAC Symposium on System Structure and Control SSSC 2016: Istanbul, Turkey, 22—24 June 2016

[40] R. Ali, P. Yunfeng, M. Touseef Iqbal, R. Ul Amin, M.O. Zahid an O.I. Khan, Adaptive backstepping sliding-mode control of coaxial octorotor unmanned aerial vehicle, IEEE Access, vol. 7, pp. 27526-27534, 2019

[41] J. Lie, D. Shin, H.Ryu, D. Lee and D.H. Shin, Fault tolerant adaptive control using time-delay control scheme under motor faults of octocopter, IEEE CSC 2018, Proc. 7th IEEE Conf. on Systems and Control, Valencia, Spain, OCt. 2018.

[42] P. Niermeyer, V.S. Akkinejpalli, M. Pak, F. Holzapfel and B. Lohmann, Geometric path following control for multirotor vehicles using Nonlinear Model Predictive Control and 3D spline paths, IEEE ICUAS 2016, IEEE 2016 Inlt. Conf. on Unmanned Aircraft Systems, Alrington, Virginia, USA, June 2016.

[43] Y. Yoon, E.N. Johnson and L. Ren, Autonomous flight control for multirotors by a simple input-output linearization with nested saturation, IEEE CCTA 2018, IEEE 2018 Conference on Control Technology and Applications, Copenhagen, Denmark, Aug. 2018

[44] T. Haus, M. Orsag and S. Bogdan, A concept of non-tilting multirotor UAV based on moving mass control, IEEE ICUAS 2017, IEEE 2017 Intl. Conf. on Unmanned Aircraft Systems, June 2017, Miami, Florida, USA.

[45] J. Trachte, F. Gonzalez and A. McFadyen, Nonlinear model predictive control for a multi-rotor with heavy slug load, IEEE ICUAS 2014, IEEE 2014 Intl. Conf. on Unmanned Aircraft Systems, May 2016, Orlando, Florida, USA

[46] A. Baldini, R. Felicetti, A. Freddi, S. Longhi and A. Monteriu, Dynamic surface control of multirotor vehicles, IEEE ICUAS 2018, IEEE 2018 Intl. Conf. on Unmanned Aircraft Systems, Dallas, Texas, USA, June 2018

[47] T. Konrad and D. Abei, A flatness-based control strategy for multirotors in industrial applications, 12th IFAC Symposium on Robot Control SYROCO 2018 Budapest, Hungary, 27–30 August 2018.

[48] C. Yao, J. Krieglstein and K. Janschek, Modelling and sliding-mode control of a fully actuated multirotor with tilted propellers, IFAC Conf. 2018

[49] G. Rigatos, P. Siano and M. Abbaszadeh, A nonlinear optimal control approach for the autonomous octorotor, Advanced Control for Applications, J. Wiley, vol. 2, no. 3, pp. 1-20, 2020

[50] G. Rigatos and P. Siano, Control of quadrotors with the use of the Derivative-free nonlinear Kalman Filter, Intelligent Industrial Systems, Springer, vol. 1, pp. 275-287, 2015.

[51] L. Shi, N. Kinkaid and J. Katupitiya, Robust control for satellite attitude regulation during on-orbit assembly, IEEE Transactions on Aerospace Science and Electronic Systems, vol. 52, no. 1, pp. 49-59, 2016

[52] T. Jiang, K. Khorasani and S. Tafazoli, Parameter estimation-based fault detection, isolation and recovery for nonlinear satellite model, IEEE Transactions on Control Systems Technology, vol. 16, no. 4, pp. 799-808, 2008.

[53] G Rigatos, M Abbaszadeh, K Busawon, L Dala, A nonlinear optimal control method for attitude stabilization of micro-satellites, Journal of Guidance, Navigation and Control, World Scientific, 2022

[54] K.W. Lee and S.N. Singh, Attractive manifold-based adaptive solar attitude control of satellites in elliptic orbits, Acta Astronautica, Elsevier, vol. 68, pp. 185-196, 2011.

[55] N.M. Horri, P. Palmer and M. Roberts, Gain-scheduled inverse optimal satellite attitude control, IEEE Transactions of Aerospace and Electronic Systems, vol. 48, no. 3, pp. 2437-2457, 2012.

[56] T.R. Patel, K.D. Kumar and K. Behdinan, Variable structure control for satellite attitude stabilization on elliptic orbits suing solar radiation pressure, Acta Astronautica, Elsevier, vol. 64, pp. 359-373, 2009.

[57] Q. Hu, L. Xiao and C. Wang, Adaptive fault-tolerant attitude tracking control for spacecraft with time-varying inertia uncertainties, Chinese Journal of Aeronautics, Elsevier, vol. 32, no. 3, pp. 674-687, 2019

[58] C. Han, J. Guo and A. Pechev, Nonlinear $H_\infty$-based underactuated attitude control for small satellites with two reaction wheels, Acta Astronautica, Elsevier, vol. 194, pp. 159-172, 2014.

[59] R. Rodrigues, A. Murillo, R. Vilela-Lopes and L.C. Cadelh de Souza, Hardware in the Loop Simulation for Model Predictive Control Applied to Satellite Attitude Control, IEEE Access, vol. 7, pp. 157401-157416, 2019.

[60] C. Han and A.N. Pechev, Underactuated satellite attitude control with two parallel CMGs, IEEE 2007 Intl. Conference on Control and Automation, Guangzhou, China, May 2007

[61] S. Ahmed and E.C. Kerrigan, Supoptimal Predictive control for satellite detumbling, Journal of Guidance, Control and Dynamics, vol. 37, No 3, pp. 850-859, 2014.

[62] Q. Wu and M. Saif, Neural adaptive observer-based fault detection and identification for satellite attitude control systems, IEEE ACC 2005, IEEE 2005 American Control Conference, Portland, Oregon, USA, July 2005.

[63] S. Singh and A Iyer, Nonlinear decoupling sliding-mode control and attitude control of spacecraft, IEEE Transactions on Aerospace and Electronic Letters, vol. 25, no. 5, pp. 621-633, 1989

[64] L.D. Yang an Y.P. Sun, Mixed $H_2/H_\infty$ state feedback design for micro-satellite attitude control, Control Engineering Practice, Elsevier, vol. 10, pp. 951-970, 2002.

[65] B. Xiao, L. Cao and D. Ram, Attitude exponential stabilization control of rigid bodies via disturbance observer, IEEE Transactions on Systems, Man and Cybernetics: Systems, 2019.

[66] A.V. Doroshin, Attitude dynamics of gyrostat-satellites under control by magnetic actuators at small perturbations, Conmunications in Nonlinear Science and Numerical Simulation, Elsevier, vol. 49, pp. 159-175, 2017

[67] Y. Yoshimoto, T. Matsuno and S. Hokamoto, Position and attitude control of an underactuated satellite with constant thrust, AIAA Guidance, Navigation, and Control Conference, Portland, Oregon, USA, Aug. 2011

[68] A. Giuseppi, A. Pietrabissa, S. Cilione and L. Galvani, Feedback linearization-based satellite attitude control woth a life-support device without communications, Control Engineering Practice, Elsevier, vol. 90, pp. 221-230, 2019

[69] C.D. Petersen, F. Leve and J. Kolmanovsky, Model Predictive Control of an underactuated spacecraft with two reaction wheels, Journal of Guidance, Control and Dynamics, vol. 40, no. 2, pp. 320-333, 2017.

[70] L. Cao, X.Q. Chen, and T. Sheng, Fault tolerant small satellite attitude control using adaptive non-singular terminal sliding modes, Advances in Space Research, Elsevier, vol. 51, pp. 2374-2393, 2013

[71] L.L. Show, J.C. Juang and Y.W. Jan, An LMI-based nonlinear attitude control approach, IEEE Transactions on Control Systems Technology, vol. 11, no. 1, pp. 73-83, 2014.

[72] C. Xue, S. Tan and H. Liu, An improved iterative sliding-mode control for tethered satellite, Proc. of the 36th Chinese Control Conference, Dalian, China, July 2012

[73] X. Liang, G. Wang, C. Hu and C. Dong, Observer-based H-infinity fault tolerant attitude control for satellite with actuator sensor faults, Journal of Aerospace Science and Technology, Elsevier, vol. 95, 2019.

[74] G. Rigatos, M. Abbaszadeh, K. Busawon and L. Dala, A nonlinear optimal control method for attitude stabilization of micro-satellites, Journal of Guidance, Navigation and Control, World Scientific, 2022

[75] G. Rigatos, P. Wira, M. Abbaszadeh, K. Busawon and L. Dala, Nonlinear optimal control autonomous hypersonic vehicles. Aerospace Systems, Springer, vol. 2, pp. 197-213, 2019